https://doi.org/10.5194/egusphere-2026-1387
Preprint. Discussion started: 24 March 2026

Feasibility of Measuring Volcanic Gas Composition Using Sky-scattered Sunlight and FTIR Spectroscopy

Tobias D. Schmitt[1,*], Moritz Sindram[2,*], Benedikt A. Löw[2], Lukas Weis[2], Ralph Kleinschek[2], Nicole Bobrowski[2,3], and André Butz[2,4,5]

[1]Kirchhoff Institute for Physics (KIP), Heidelberg University, Germany
[2]Institute of Environmental Physics (IUP), Heidelberg University, Germany
[3]Istituto Nazionale di Geofisica e Vulcanologia, Osservatorio Etneo, Catania, Italy
[4]Heidelberg Center for the Environment (HCE), Heidelberg University, Germany
[5]Interdisciplinary Center for Scientific Computing (IWR), Heidelberg University, Germany
[*]These authors contributed equally to this work.

Correspondence: Tobias D. Schmitt (tobias.schmitt@kip.uni-heidelberg.de), Moritz Sindram (msindram@iup.uni-heidelberg.de), André Butz (andre.butz@uni-heidelberg.de)

Abstract. Monitoring volcanic emissions is essential for understanding volcanic processes and predicting eruption dynamics. Remote sensing is the only method that allows safe measurements right before, during, and after eruptions. Current monitoring is mostly limited to the ultraviolet and visible (UV-VIS) spectral ranges due to the high sky brightness in that region, restricting observations largely to SO_2.

Here, we assess the feasibility of constraining volcanic emissions using passive Fourier transform infrared (FTIR) spectroscopy of sky-scattered sunlight in the near-infrared (NIR), where absorption features of a broader range of gases of interest are available. Using an instrument model for spectral signal-to-noise ratio (SNR) combined with an information-content analysis, we estimate detection limits for individual trace gas columns under realistic conditions. To address systematic uncertainties always present in atmospheric total column measurements, we developed an innovative approach of incorporating actual measurements into our estimations. The instrument model accurately reproduced laboratory validation experiments. To assess applicability of the method, this study focuses on Mount Etna as a representative high-emission volcano. Our results indicate that CO_2 column measurements remain challenging. Even under bright sky conditions, measurement times of 30 minutes are necessary to reach detection limits on the scale of the expected total column enhancement. This renders flux estimations via plume transects not feasible, while plume-composition measurements might be possible. In contrast, strongly emitted halogen species such as HCl and HF are detectable within tens of seconds under bright skies and up to approximately 10 minutes for dark conditions, owing to their low atmospheric background concentrations. The limitations identified for CO_2 are largely independent of the specific spectroscopic implementation, since they arise fundamentally from the low amount of available light. Finally, the SNR and detection-limit analysis using actual measurements is broadly applicable to other instruments, spectral regions, and target species.

https://doi.org/10.5194/egusphere-2026-1387
Preprint. Discussion started: 24 March 2026

1 Introduction

Volcanic gases are central to eruption dynamics, with their flux composition providing insights into subsurface processes. Further, once released into the atmosphere, these gases influence atmospheric composition and climate, although the global volcanic fluxes remain poorly constrained. Only remote sensing methods allow measurements of gases from a safe distance, also during high volcanic activity.

Already in the 19th century, Judd (1895) suggested that spectroscopy could provide an important tool in volcanology. Verhoogen (1939) performed the first successful spectroscopic gas measurements, using light in the visible range. Delsemme and Évrard (1960) and Murata (1960) performed the first measurements in the NIR at Kilauea and Nyiragongo, respectively, with both being able to detect CuCl in the volcanic gas plumes. In the late 1960s Naughton et al. (1969) succeeded in determining the major gas composition by using infrared absorptions between 2.5 to 14.5 μm and the light from a lava fountain of Kilauea volcano, Hawaii, United States. The authors were the first to determine the main components of a volcanic plume by remote sensing measurements, namely the contributions of H_2O, CO_2, SO_2.

The commercial availability of rugged, compact Fourier transform infrared (FTIR) spectrometers in the 1990s allowed for more frequent volcanological applications of IR spectroscopy (e.g., Notsu et al., 1993; Mori et al., 1993; Francis et al., 1998; Oppenheimer et al., 1998). Operating in the infrared region (500–6000 cm^{-1}) at spectral resolutions of up to 0.5 cm^{-1}, these devices opened up the possibility of measuring many volcanic species of interest (including HCl, H_2O, SO_2, HF, CO_2, SiF_4, OCS, and CO) using their rotation-vibration line structures. Today, several research groups use IR spectroscopy to investigate volcanic degassing and have contributed to advancing our understanding of volcanic processes (e.g., Allard et al., 2005; Burton et al., 2007; Scott et al., 2023; Smekens et al., 2024).

However, IR remote sensing measurements are still seldom employed for volcanic monitoring, i.e., ideally continuous and automated observations. The instruments are typically deployed in stationary positions on the ground and pointed at a hot source, for example, an infrared lamp, the crater, or the Sun. The availability of this light source is the most serious limitation encountered in deployment: The number of active lava domes and lava fountains is small, and using them limits the measurement temporally to times during the eruptions. The usage of direct sunlight is in many places unreliable, and the sun is rarely in the correct geometric relationship to plume and instrument, resulting in considerable effort when measuring plume transects (Butz et al., 2017). There were a few attempts to take advantage of IR emission spectroscopy using the thermal emissions of the volcanic gas itself (Love et al., 1998; Goff et al., 2001), but these remained isolated case studies.

Successful monitoring nowadays mainly relies on scattered sunlight in the UV region (Galle et al., 2003; Burton et al., 2009; Galle et al., 2010; Burton et al., 2015; Arellano et al., 2021). The usage of scattered sunlight comes with the advantage of not limiting the measurements to clear sky conditions and resolves many geometric restrictions. But these monitoring efforts are mostly limited to SO_2, since other gases of interest lack suitable absorption features in the UV-VIS region, where plenty of scattered light is available. The question is whether the comparatively low intensity of scattered sunlight in the NIR region is sufficient for measurements of gases of interest to volcanology which have characteristic absorption lines there (e.g., H_2O, CO_2, HCl, HF, etc.).

https://doi.org/10.5194/egusphere-2026-1387
Preprint. Discussion started: 24 March 2026

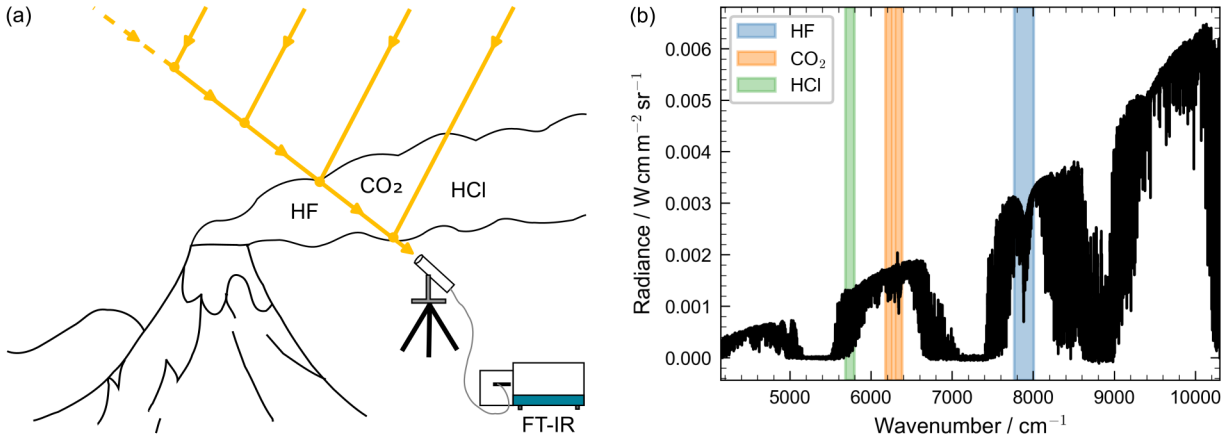

Figure 1. Measurement concept of plume composition using sky scattered sunlight. (a) Sketch of a measurement of sky-scattered sunlight at a volcano and contributing light paths for a certain viewing direction. (b) Spectrum of sky-scattered sunlight taken with the EM27/SCAv2 instrument in the same measurement geometry in Heidelberg.

Section 2 introduces the concepts of measuring volcanic emissions by spectroscopy of sky-scattered sunlight. Section 3 presents the instrument used in this study, as well as proposed changes to optimize for volcano measurements. Section 4 presents the predicted measurement performance of an optimized FTIR setup in the NIR region. This includes the prediction of spectroscopic performance (i.e., signal-to-noise ratio (SNR) of a single spectrum) as well as the resulting precision of retrieved trace gas columns for different target gases. Finally, Sect. 5 summarizes and concludes our findings.

2 Measuring volcanic plumes using sky scattered sunlight

We describe here an instrument concept that exploits spectra of sky-scattered sunlight in the NIR spectral region. A telescope collects light from a chosen viewing direction (Fig. 1a) and forwards it to spectrometer for analysis (Fig. 1b). The instrument or a separate telescope collects light in a certain viewing direction (Fig. 1a), which is then spectroscopically analyzed (Fig. 1b). A fitting routine retrieves the total-column abundance of the target trace gases, e.g., CO_2, HF, HCl, and provides ancillary information such as water-vapor content or total air mass, the latter derived from the O_2 column.

By acquiring a series of measurements while scanning across the plume of an emission source, e.g., a volcano, we can infer the plume's target-gas enhancement and its spatial profile. These data, in turn, constrain the source's total emissions (e.g., Galle et al., 2010; Burton et al., 2015; Kern et al., 2015; Arellano et al., 2021; Knapp et al., 2024). Alternatively, when the plume's location is known a priori, measurements taken on-axis and off-axis provide direct information on plume composition.

The NIR spectral range offers a distinct advantage for these measurements: although its absorption features are generally weaker and the set of detectable species is smaller than in the MIR, Rayleigh and Mie scattering are stronger at shorter wavelengths, yielding a considerably brighter background signal.

https://doi.org/10.5194/egusphere-2026-1387
Preprint. Discussion started: 24 March 2026

3 Instruments utilized in this study

For laboratory-verification and reference measurements of sky-scattered sunlight we employ an existing FTIR instrument that was originally developed for ground-scattered sunlight and is the successor of the instrument presented in Löw et al. (2023). In this work we refer to it as the **EM27/SCAv2**. The spectrometer is equipped with a Hamamatsu G12183-210KA-03 InGaAs photodiode, cooled by a two-stage thermoelectric (TE) cooler. Spectral fitting is performed with a customized version of the RemoTeC algorithm (Butz et al., 2011), further modified for ground-based scattered-sunlight measurements (Löw et al., 2023). A schematic of the instrument's internal layout is shown in Fig. A1.

To assess how such a system could perform for volcanic plume observations, we devised a second instrument version that is specifically optimized for the anticipated measurement conditions. For the purpose of this study we designate it **EM27/Volcano**. The principal modification is the substitution of the detector with a Hamamatsu G12181-210K photodiode. This device exhibits a higher responsivity around the target wavelength of 1.6 µm and possesses substantially larger shunt resistance owing to its narrower spectral bandwidth.

The narrower bandwidth means that the strong CO_2 absorption bands near 2 µm are no longer accessible. However, synthetic performance studies, similar in spirit to the analysis presented here but beyond the scope of this article, indicate that the resulting increase in spectral SNR more than compensates for the loss of the 2 µm lines. Consequently, the EM27/Volcano detector choice is expected to deliver the best overall CO_2 performance for volcanic plume measurements.

4 Prediction of measurement performance and limits

The prediction of the overall measurement performance consists of two, largely independent parts: (i) an estimation of the quality of the optical measurement itself, and (ii) an information content analysis, which links the spectral performance to the measurement target, i.e., the retrievable trace gas columns.

In the first component, we estimate the spectral signal-to-noise ratio (SNR) using an instrument model based on fundamental principles of optics and detector electronics, complemented by FTIR-specific characteristics.

The second component translates the achievable SNR into trace gas retrieval performance using an information content analysis. For this purpose, we select Mount Etna as a test case. It is one of the largest halogen point sources on Earth (Aiuppa et al., 2005), among the strongest volcanic emitters of CO_2 (Aiuppa et al., 2019), and one of the most significant continuous emitters of volcanic gases worldwide (Pyle and Mather, 2009). In addition, the results of Butz et al. (2017) provide a benchmark for expected gas column enhancements at Mount Etna, and radiometrically calibrated measurements of sky radiances were available to us to constrain our simulations. This use of real observations allows us to also consider systematic effects, which typically occur for total column measurements of trace gases.

Section 4.1 describes the instrument model and SNR estimation. Section 4.2 presents a laboratory validation of the model. Section 4.3 reports on the information content analysis and links spectral SNR to the precisions of trace gas column densities. Finally, Sect. 4.4 brings all the steps together and delivers the final assessment of the trace gas performance in the volcano setting.

https://doi.org/10.5194/egusphere-2026-1387
Preprint. Discussion started: 24 March 2026

Table 1. Summary of the instrument parameters and their symbols.

instrument part	parameter name	symbol	unit
input	radiance	$L_\mathrm{e}(\tilde{\nu})$	$\frac{\mathrm{W}}{\mathrm{cm}^{-1}\,\mathrm{sr}\,\mathrm{m}^2}$
optics	transmission	$\tau(\tilde{\nu})$	1
	étendue	E	sr m^2
detector	responsivity	$R(\tilde{\nu})$	$\frac{\mathrm{A}}{\mathrm{W}}$
	shunt resistance	R_shunt	Ω
	temperature	T	K
digitization	maximal OPD	$\mathrm{OPD}_\mathrm{max}$	cm
	scanning speed	f_scan	Hz
	reference wavenumber	$\tilde{\nu}_\mathrm{ref}$	cm^{-1}

4.1 Instrument model and prediction of spectrometer performance

The instrument model for our FTIR measurement needs to address the three main systems of our instrument: First, the optics, which deliver the optical power to the detector. Second, the detector and its front-end, which convert the optical power into an electrical signal, but can also introduce noise. And finally, the sampling and digitization of the signal, which defines the resolution, noise bandwidth, and acquisition time. Table 1 lists all instrument parameters relevant to the instrument model. The following calculations are based on fundamental laws of optics and electronics, as well as, the basic measurement concept of FTIR spectroscopy. Both are documented in many textbooks, e.g., Hobbs (2009) and Griffiths and De Haseth (2007).

First, we determine the average spectral power on the detector $P(\tilde{\nu})$, as a function of the wavenumber $\tilde{\nu}$. This is given by the product of the source radiance $L_\mathrm{e}(\tilde{\nu})$, the transmission of all the optics combined $\tau(\tilde{\nu})$, the geometric light throughput of the system E, also called étendue, and a factor $1/2$ due to the ideal average transmission of the interferometer:

$$P(\tilde{\nu}) = \frac{1}{2} L_\mathrm{e}(\tilde{\nu}) \tau(\tilde{\nu}) E \tag{1}$$

The average power on the detector and the responsivity of the detector $R(\tilde{\nu})$ itself gives rise to an average photo current:

$$I_\mathrm{ph} = \int P(\tilde{\nu}) R(\tilde{\nu}) \, \mathrm{d}\tilde{\nu} \tag{2}$$

The dominant noise in the front-end can be of different origin; ideally, it is the unavoidable shot noise, but for low-light measurements, the thermal noise of the diode's shunt resistance or the gain resistance might be dominant. In our case and parameter space, the thermal noise of the shunt resistance dominates at low light conditions, and shot noise becomes increasingly relevant for brighter scenes. Their respective noise spectral densities S are given by the following equations, where k_b is the

https://doi.org/10.5194/egusphere-2026-1387
Preprint. Discussion started: 24 March 2026

Boltzmann constant, T the temperature of the diode, R_{shunt} its shunt resistance, and e the elementary charge:

$$S_{\mathrm{shunt}} = \frac{4k_{\mathrm{b}}T}{R_{\mathrm{shunt}}} \tag{3}$$

$$S_{\mathrm{shot}} = 2eI_{\mathrm{ph}} \tag{4}$$

They are essentially power quantities (units of A^2/Hz) which is also why the photo current appears linear in the expression for the shot noise. Also, they directly add to the total noise spectral density S_{tot}:

$$S_{\mathrm{tot}} = S_{\mathrm{shunt}} + S_{\mathrm{shot}} \tag{5}$$

Now, with a description of the signal power and detector noise, we address the digitization and processing. An FTIR instrument digitizes the signal as a function of optical path difference (OPD) up to a maximum ($\mathrm{OPD}_{\mathrm{max}}$), which results after a Fourier transform in a spectral bandwidth (or spectral sampling) $\Delta\tilde{\nu}$ of

$$\Delta\tilde{\nu} = \frac{1}{\mathrm{OPD}_{\mathrm{max}}}. \tag{6}$$

The instrument scans the OPD at an optical speed of $f_{\mathrm{scan}}/\tilde{\nu}_{\mathrm{ref}}$, where $\tilde{\nu}_{\mathrm{ref}}$ is the wavenumber of the reference laser of the instrument and f_{scan} is the frequency of its resulting modulation in the interferometer at the set speed of the scanner. We keep to the convention to call the modulation frequency of the reference laser f_{scan} "scanning speed", even though for those unfamiliar with FTIR spectroscopy, it might be irritating to call a frequency "speed". Using the above definition, the time of a single acquisition t_0 is given by

$$t_0 = \frac{\mathrm{OPD}_{\mathrm{max}}\,\tilde{\nu}_{\mathrm{ref}}}{f_{\mathrm{scan}}} = \frac{1}{\Delta f} \tag{7}$$

and defines the equivalent bandwidth of a spectral bin in frequency space Δf accordingly. Assuming that $P(\tilde{\nu})$ and $R(\tilde{\nu})$ vary slowly on the scale of $\Delta\tilde{\nu}$, the signal current for a spectral bin $i_{\mathrm{sig}}(\tilde{\nu})$ is defined by

$$i_{\mathrm{sig}}(\tilde{\nu}) = P(\tilde{\nu})\,R(\tilde{\nu})\,\Delta\tilde{\nu} \tag{8}$$

and the corresponding noise current by

$$i_{\mathrm{noise}} = \sqrt{S_{\mathrm{tot}}\,\Delta f}. \tag{9}$$

The spectral SNR of a single spectrum is now given by $i_{\mathrm{sig}}(\tilde{\nu})/i_{\mathrm{noise}}$ and the SNR of a measurement acquired over a measurement time t and averaged over $N = t/t_0$ single acquisitions is

$$\mathrm{SNR}(\tilde{\nu}) = \frac{i_{\mathrm{sig}}(\tilde{\nu})}{i_{\mathrm{noise}}}\sqrt{N} = \frac{P(\tilde{\nu})\,R(\tilde{\nu})}{\sqrt{S_{\mathrm{tot}}}}\,\frac{\sqrt{t}}{\mathrm{OPD}_{\mathrm{max}}} = \underbrace{L_{\mathrm{e}}(\tilde{\nu})}_{\text{term A}}\,\underbrace{\frac{\tau(\tilde{\nu})E\,R(\tilde{\nu})}{2\sqrt{S_{\mathrm{tot}}}}}_{\text{term B}}\,\underbrace{\frac{\sqrt{t}}{\mathrm{OPD}_{\mathrm{max}}}}_{\text{term C}}. \tag{10}$$

Term C in Eq. 10 contains parameters which are, to some extent, a choice of the user and demonstrates the typical trading rules of (FTIR) spectroscopy: SNR improves with the square root of the number of averaged measurements, i.e., the measurement

https://doi.org/10.5194/egusphere-2026-1387
Preprint. Discussion started: 24 March 2026

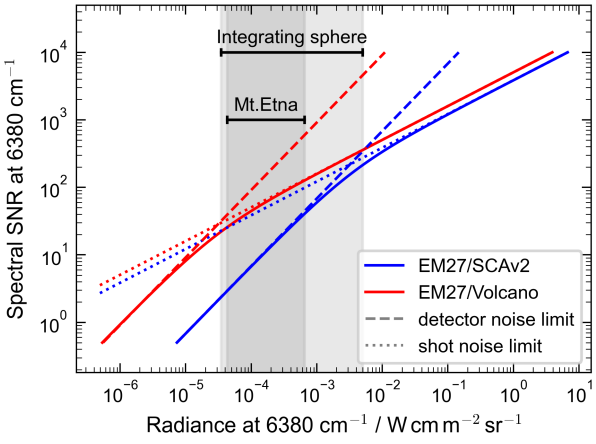

Figure 2. Spectral SNR changing with increasing radiance (at 6380 cm^{-1}) for two different sets of instrument parameters. One matches the EM27/SCAv2, the instrument used for the laboratory verification in Sect. 4.2 and one the EM27/Volcano, which is optimized for low radiance conditions. The total photo current is calculated assuming a typical spectrum like in Fig. 1b. The transition from a detector-noise-limited regime at low radiances to a shot-noise-limited regime is clearly visible for both parameter sets. The shaded areas give the range of radiances expected at Mount Etna, Italy and emitted by the integrating sphere in the verification experiment of Sect. 4.2.

time, and decreases linearly with improved resolution, i.e., increased $\mathrm{OPD}_{\max}$. On the other hand, term B in Eq. 10 contains all fixed instrument parameters that are either available or can be easily estimated: The detector's responsivity can be obtained from its data sheet or that of a similar detector. The same is true for transmissions and reflectivities of beam splitter, windows, and mirrors. The only exception to this is the noise spectral density, which might depend in a relevant way on the input radiance if we are in or near the shot-noise-limited regime. Finally, term A in Eq. 10 represents the linear increase of signal strength with increasing signal power, i.e., increasing input radiance $L_{\mathrm{e}}(\tilde{\nu})$. Figure 2 illustrates the SNR as a function of input radiance (using a typical radiance profile and scaling it in intensity). At low radiance levels, the relationship between spectral SNR and radiance is linear. For high radiances, spectral SNR rises only with the square root of the input radiance, since the noise spectral density S_{tot} is dominated by shot noise and grows linearly with the radiance.

The radiance can be the most difficult parameter to estimate, depending on the application. For artificial light sources, consulting the data sheet might already provide a sufficient estimate. For sky-scattered sunlight, it is possible to obtain a lower boundary by assuming black body radiation for the sun's spectrum and calculating Rayleigh scattering in a single-scattering approximation. An upper bound can be obtained by repeating the calculation with Mie scattering and a high assumed aerosol load. In our case, we had sufficiently calibrated measurements of the sky brightness, which informed us of a realistic range of radiances.

Finally, a brief remark on the choice of apodization. All the above calculations ignore apodization, i.e., assume a "box-car" apodization and are correct for this case. When working with any other apodization function, for example, one of the Norton-Beer functions, this suppresses high-frequency contributions, consequently reducing the apparent noise when measured by

https://doi.org/10.5194/egusphere-2026-1387
Preprint. Discussion started: 24 March 2026

taking a standard deviation and improving the baseline SNR. This apparent increase in SNR is, of course, not a real information gain, as apodization also weakens the spectroscopic features. So when using the definition of baseline SNR and apodization, the SNR prediction needs to be scaled by an additional factor that accounts for this and depends on the exact functions (e.g., $\sqrt{3}$ for triangular apodization or 1.58 for the Norton-Beer medium function.)

4.2 Experimental validation of the instrument model

To assess the predictive capability of the instrument model presented in Section 4.1, we carried out a straightforward laboratory test. First, we measured the radiance emitted from an integrating sphere with a calibrated spectrometer. Next, the obtained radiance spectrum, together with an expected value range for each model parameter, served as input for the instrument model to compute the expected SNR interval for the device under test, the EM27/SCAv2.

Subsequently, we measured the same radiance emitted from the integrating sphere with the device under test and extracted the actual SNR from the spectrum. We repeated the procedure for seven different source brightness levels, deliberately spanning the transition from shot-noise-limited to detector-noise-limited operation. Because raising the power supplied to the halogen lamps changes not only the overall intensity but also the shape of the spectrum, this test goes beyond a simple scaling of the spectrum shown in Fig. 2.

Figure 3 displays the results of this experiment. All measured SNR values lie within the model's predicted interval, and they follow a clear systematic trend: at low illumination, the points are biased towards the lower half of the interval, while at higher illumination, they drift toward the interval's centre. For low radiance, the width of the prediction band is dominated by uncertainties in the detector's shunt resistance and its temperature. For high radiances, in the shot-noise dominated regime, the prediction range is dominated by the total amount of photons reaching the detector, so the uncertainty in total optical transmission and étendue. This explains the gradual shift of the measured performance's relative position in the prediction interval with increasing lamp power, nicely demonstrating self-consistency.

Table A1 details the specific parameter choices that generate the prediction envelope and provides additional technical information.

4.3 Linking spectral SNR to precision of trace gas columns

Linking the spectral SNR to the precision of trace gas column densities derived from the corresponding spectrum is the final step required to predict trace gas performance from a reference radiance spectrum.

In principle, a purely synthetic study could establish this relationship by using a radiative transfer model to generate the "true" spectrum. Adding random white noise to achieve a specific SNR, and then run error propagation throught the retrieval algorithm would provide the expected precision.

In practice, however, this approach neglects systematic errors that arise, among others, from necessary simplifications in the atmospheric representation, imperfections in the spectroscopic database. To capture these real world effects we use measurements taken with the EM27/SCAv2 instrument, together with the published data and instrument performance at Mount Etna reported by Butz et al. (2017).

https://doi.org/10.5194/egusphere-2026-1387
Preprint. Discussion started: 24 March 2026

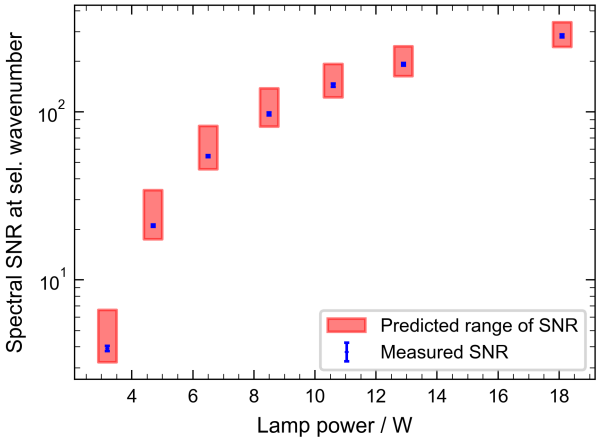

Figure 3. Comparison of measured SNR to the range predicted by the instrument model and the input parameters as a function of optical input power to the integrating sphere. At low radiances, the large prediction span is dominated by the uncertainty in detector temperature and its shunt resistance. At high radiances, the span is dominated by the total transmission of the optical elements (mirrors, etc.) and the light throughput. Table A1 provides details the specific parameter choices.

We recorded spectra of sky-scattered sunlight for 1 minute each at a viewing zenith angle (VZA) of approximately 70 °, which is reasonable for volcanic measurements. The measurements were performed in Heidelberg on the roof of the Institute of Environmental Physics (49.417342° N, 8.674536° E, 144m above sea level), starting 20 September 2024, 07:00 UTC, for about five hours. By co-adding different numbers of successive spectra, we generate a set of spectra with different SNR from the same raw data and retrieve CO_2 information. Figure 4 displays the resulting dependence of retrieval precision on SNR. The plot resembles an Allan deviation curve, but the abscissa is spectral SNR rather than averaging time.

Because spectra with high SNR were produced by extending the averaging time, the apparent degradation of CO_2 column precision at the longest averaging intervals is not a true loss of performance, but merely reflects the dominance of real atmospheric variability over pure statistical noise. In the regime where the curve follows the expected $1/\mathrm{SNR}$ trend (the first few data points), we determine a proportionality constant of $2.3 \cdot 10^{22}\,\mathrm{molec/cm^2}$.

To convert the spectral SNR into a slant column precision for HF and HCl, we cannot follow the same direct route used for CO_2, since HF and HCl are essentially absent from the spectra acquired for this study. Instead, we adopt the empirical relationship reported by Butz et al. (2017) to link HF or HCl precision to CO_2 precision, i.e.,

$$\sigma_x = \sigma_{\mathrm{CO_2}} \frac{\sigma_{x,\,\mathrm{lit}}}{\sigma_{\mathrm{CO_2},\,\mathrm{lit}}}, \tag{11}$$

where x indicates the species HF or HCl and the index lit marks values taken from Butz et al. (2017).

https://doi.org/10.5194/egusphere-2026-1387
Preprint. Discussion started: 24 March 2026

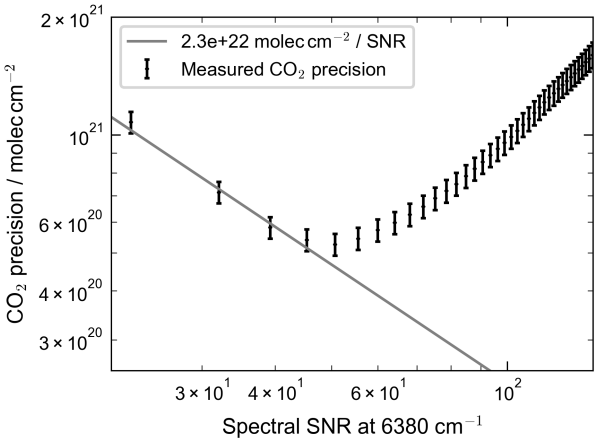

Figure 4. Relation between spectral SNR at $6380\ \mathrm{cm}^{-1}$ and the precision of the retrieved CO_2 slant column density. One-minute spectra constitute the data basis. Data points for higher spectral SNR result from averaging consecutive spectra, similar to an Allan deviation. Thus, at high spectral SNR the curve departs from the expected inverse trend because atmospheric variability dominates at longer averaging times.

4.4 Prediction of trace gas performance in a volcano setting for a given spectrometer performance

Bringing all of the pieces together, we can now predict the trace gas performances of CO_2, HF, and HCl for a volcanic measurement with an FTIR observing sky-scattered sunlight.

To estimate the input radiance, we consult radiance measurements recorded during a 2021 measurement campaign at Mount Etna, Italy, with a radiometrically calibrated grating spectrometer. We consider a clear-sky condition as the lower bound and a high-aerosol-loaded sky as the upper bound for the input radiance, both differing by about an order of magnitude in the NIR. Figure 5 shows grey-scale images of the respective scenes to illustrate the brightness in the NIR.

The EM27/Volcano, the optimized, but hypothetical instrument under consideration, uses a narrower-bandwidth detector, which shows improved responsivity at 1.6 µm and substantially higher shunt resistances, allowing for shot-noise-limited operation at lower radiances. Further, the improved responsivity, together with a long-pass filter at 1.1 µm, which reduces the relative number of non-signal photons on the detector, improves performance in the shot-noise-limited regime (see Fig. 2).

Using the instrument model developed in Sect. 4.1, in particular Eq. 10, we estimate the spectral performance for these input radiances as a function of measurement time. The results from Sect. 4.3, in particular the scaling factor derived from Fig. 4 links these to CO_2 precision, and, by scaling accordingly to the results from Butz et al. (2017), i.e., Eq. 11, to HF and HCl precisions.

Figure 6 shows these resulting trace gas performances for all species as a function of measurement time, with the shaded area spanning the range between the bright and dark sky scenarios. Horizontal dashed lines show the column enhancements measured by Butz et al. (2017) and indicate a realistic signal strength. We can infer the required measurement times to detect a typical plume enhancement from the intersections of the dashed lines with the shaded areas. These times range from

https://doi.org/10.5194/egusphere-2026-1387
Preprint. Discussion started: 24 March 2026

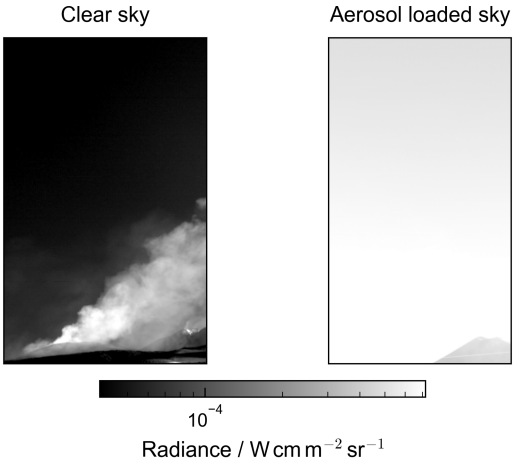

Figure 5. Grey scale images demonstrating the considered range of sky brightness at 6380 cm^{-1} in the NIR.

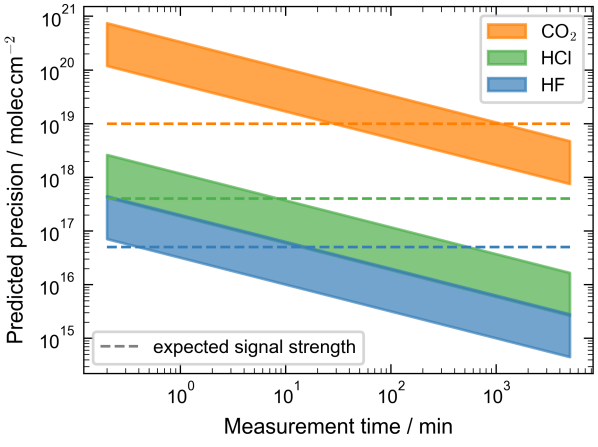

Figure 6. Predicted precision of CO_2, HCl, and HF as a function of measurement time. The shaded bars reflect from the expected range of radiances (clear-sky vs. aerosol-loaded sky). The horizontal dashed lines indicate the maximum volcanic enhancements for each species, detected by Butz et al. (2017) at Mount Etna, Italy.

approximately 30 minutes to a full day for CO_2 and from approximately 30 seconds to 20 minutes for HCl and HF, with a slightly better performance for HCl. As a result, measurements of CO_2 emissions seem unlikely, even for bright sky conditions, since plume transects consist of multiple measurements, where each individual measurement should exhibit a precision well below the expected plume enhancement. Plume-composition measurements might be feasible with additional information on the plume position, but remain challenging for unstable meterological conditions. The picture is more nuanced for HCl and HF,

https://doi.org/10.5194/egusphere-2026-1387
Preprint. Discussion started: 24 March 2026

with sufficiently low required measurement times to potentially allow for plume transect measurements, at least under bright sky conditions.

5 Conclusions

In this study, we assessed the feasibility of constraining volcanic emissions using passive spectroscopy of sky-scattered sunlight in the NIR. We developed an instrument SNR model, validated it with laboratory measurements, and combined it with an information-content analysis to estimate detection limits for trace gas columns under realistic conditions.

Our results indicate that reliably measuring CO_2 columns in volcanic plumes remains challenging. Even under bright sky conditions, the SNR is insufficient to resolve typical plume enhancements with the precision required for robust flux estimates. As a result, constraining CO_2 emissions via plume transects would likely require alternative observational strategies or measurement concepts.

In contrast, halogen species such as HCl and HF are detectable at volcanoes with high emissions. Their low atmospheric background concentrations result in substantially higher signal-to-background ratios, making the proposed method a valid approach for these species, at least for bright sky conditions. Combined with information on the plume position, e.g., from SO_2-cameras, plume-composition measurements might be possible also in less favourable conditions.

Based on these findings, we did not pursue construction of the optimized EM27/Volcano instrument. The limitations arise fundamentally from the limited amount of scattered NIR light and are largely independent of the specific spectroscopic implementation (FTIR in this study). Any method aiming to overcome this limitation would likely need to either collect substantially more light, restrict observations to a narrow spectral region around the CO_2 lines to increase the ratio of signal photons to irrelevant background photons, or combine both approaches. A meaningful increase to the light throughput appears unlikely, as the proposed instrument already utilizes 2-inch optics and there are no suitable FTIR platforms with larger optics commercially available. Also, the added size and mass would make the instrument too bulky and heavy for field deployment. Restricting the spectral range, however, introduces additional challenges: it can complicate baseline estimation and reduces the information available to characterize scattering in the retrieval.

Finally, while the physical principles used in the analysis are well known, the combination of SNR modeling with information content assessment provides a quantitative evaluation that is not always straightforward to implement in practice. Especially systematic effects, that are hard to capture in a purely synthetic study, remain challenging to incorporate correctly. Our approach in this study of incorporating actual data into the process provides a solution to this issue which is generally applicable to other instruments, spectral regions, target species, and measurement scenarios, and could guide future feasibility studies or the development of improved measurement concepts.

Code availability. The software is available from the authors upon request.

https://doi.org/10.5194/egusphere-2026-1387
Preprint. Discussion started: 24 March 2026

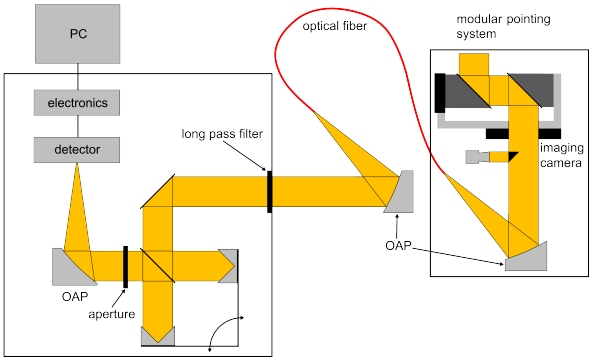

Figure A1. Schematic of the EM27/SCAv2 instrument. On the right side is a modular pointing system in a robust and weatherproof housing. It couples the captured light into an optical fiber and guides it to the spectrometer (on the left). In the spectrometer, the light is modulated by the interferometer and imaged on the photodiode/detector. The front-end and sampling electronics process and digitize the signal and send it to the PC. The imaging camera in the pointing system enables precise aiming and monitoring.

Table A1. Hardware parameters used in the instrument model and their assumption-derived value ranges that produce the prediction interval shown in Fig. 3. The total transmission efficiency of the optics combines the losses from mirrors, windows, filters, the optical fiber, and the beam splitter. For the étendue, the field of view is fixed by the focal length (101.6 mm) and the detector diameter (1 mm), but the assumed usable beam cross-sectional area varies.

instrument part	parameter name	symbol	span
optics	transmission	$\tau(\tilde{\nu})$	$0.52 - 0.67$
	étendue	E	$(0.304 - 0.345)$ sr mm^2
detector	responsivity	$R(\tilde{\nu})$	according to data sheet
	shunt resistance	R_{shunt}	$(200 - 400)$ kΩ
	temperature	T	$(240 - 250)$ K
digitization	maximal OPD	$\mathrm{OPD}_{\mathrm{max}}$	1.8 cm

Author contributions. MS performed all measurements and carried out the formal data analysis. TDS and MS developed the instrument model. BAL provided the reference instrument and its radiometric calibration. BAL supported the analysis for the full-physics retrieval. LW developed and built the current version of the instrument with RK and BAL supporting the process. NB supported the project with her expertise in volcano field measurements. TDS, MS, and NB wrote the paper, and all authors commented on the draft. TDS conceptualized the feasibility study and the experimental validation of the instrument model. AB supervised the study and hypothesized that volcanic CO2 measurements in sky-scattered sunlight are possible.

Competing interests. At least one of the Authors is a member of the editorial board of Atmospheric Measurement Techniques.

https://doi.org/10.5194/egusphere-2026-1387
Preprint. Discussion started: 24 March 2026

Acknowledgements. Special thanks go to Marvin Knapp for recording the NIR measurements of the sky at Mount Etna with the Hyspex instrument during a measurement campaign in Summer 2021. Their availability made this study more straightforward and more robust. Further, the authors acknowledge the usage of large language model based AI tools to assist in drafting, revising, and developing material related to this manuscript. All AI-generated output, including text and plotting scripts, was critically reviewed, edited, and validated by the authors, who take full responsibility for the final content.

https://doi.org/10.5194/egusphere-2026-1387
Preprint. Discussion started: 24 March 2026

References

Aiuppa, A., Federico, C., Franco, A., Giudice, G., Gurrieri, S., Inguaggiato, S., Liuzzo, M., McGonigle, A. J. S., and Valenza, M.: Emission of Bromine and Iodine from Mount Etna Volcano, Geochem. Geophy. Geosy., 6, 2005GC000 965, https://agupubs.onlinelibrary.wiley.com/doi/10.1029/2005GC000965, 2005.

Aiuppa, A., Fischer, T. P., Plank, T., and Bani, P.: CO2 Flux Emissions from the Earth's Most Actively Degassing Volcanoes, 2005–2015, Sci. Rep., 9, 5442, https://www.nature.com/articles/s41598-019-41901-y, 2019.

Allard, P., Burton, M., and Muré, F.: Spectroscopic Evidence for a Lava Fountain Driven by Previously Accumulated Magmatic Gas, Nature, 433, 407–410, https://www.nature.com/articles/nature03246, 2005.

Arellano, S., Galle, B., Apaza, F., Avard, G., Barrington, C., Bobrowski, N., Bucarey, C., Burbano, V., Burton, M., Chacón, Z., Chigna, G., Clarito, C. J., Conde, V., Costa, F., De Moor, M., Delgado-Granados, H., Di Muro, A., Fernandez, D., Garzón, G., Gunawan, H., Haerani, N., Hansteen, T. H., Hidalgo, S., Inguaggiato, S., Johansson, M., Kern, C., Kihlman, M., Kowalski, P., Masias, P., Montalvo, F., Möller, J., Platt, U., Rivera, C., Saballos, A., Salerno, G., Taisne, B., Vásconez, F., Velásquez, G., Vita, F., and Yalire, M.: Synoptic Analysis of a Decade of Daily Measurements of SO_2 Emission in the Troposphere from Volcanoes of the Global Ground-Based Network for Observation of Volcanic and Atmospheric Change, Earth Syst. Sci. Data, 13, 1167–1188, https://essd.copernicus.org/articles/13/1167/2021/, 2021.

Burton, M., Allard, P., Muré, F., and La Spina, A.: Magmatic Gas Composition Reveals the Source Depth of Slug-Driven Strombolian Explosive Activity, Science, 317, 227–230, https://www.science.org/doi/10.1126/science.1141900, 2007.

Burton, M., Caltabiano, T., Murè, F., Salerno, G., and Randazzo, D.: SO_2 Flux from Stromboli during the 2007 Eruption: Results from the FLAME Network and Traverse Measurements, J. Volcanol. Geoth. Res., 182, 214–220, https://linkinghub.elsevier.com/retrieve/pii/S0377027308006240, 2009.

Burton, M., Salerno, G., D'Auria, L., Caltabiano, T., Murè, F., and Maugeri, R.: SO_2 Flux Monitoring at Stromboli with the New Permanent INGV SO_2 Camera System: A Comparison with the FLAME Network and Seismological Data, J. Volcanol. Geoth. Res., 300, 95–102, https://linkinghub.elsevier.com/retrieve/pii/S0377027315000396, 2015.

Butz, A., Guerlet, S., Hasekamp, O., Schepers, D., Galli, A., Aben, I., Frankenberg, C., Hartmann, J.-M., Tran, H., Kuze, A., Keppel-Aleks, G., Toon, G., Wunch, D., Wennberg, P., Deutscher, N., Griffith, D., Macatangay, R., Messerschmidt, J., Notholt, J., and Warneke, T.: Toward Accurate CO_2 and CH_4 Observations from GOSAT: GOSAT CO_2 and CH_4 Validation, Geophys. Res. Lett., 38, n/a–n/a, http://doi.wiley.com/10.1029/2011GL047888, 2011.

Butz, A., Dinger, A. S., Bobrowski, N., Kostinek, J., Fieber, L., Fischerkeller, C., Giuffrida, G. B., Hase, F., Klappenbach, F., Kuhn, J., Lübcke, P., Tirpitz, L., and Tu, Q.: Remote Sensing of Volcanic CO_2, HF, HCl, SO_2, and BrO in the Downwind Plume of Mt. Etna, Atmos. Meas. Tech., 10, 1–14, https://amt.copernicus.org/articles/10/1/2017/, 2017.

Delsemme, A. H. and Évrard, P.: Spectroscopie de Flammes Volcaniques, Centre National de Volcanologie, 1960.

Francis, P., Burton, M. R., and Oppenheimer, C.: Remote Measurements of Volcanic Gas Compositions by Solar Occultation Spectroscopy, Nature, 396, 567–570, https://www.nature.com/articles/25115, 1998.

Galle, B., Oppenheimer, C., Geyer, A., McGonigle, A. J., Edmonds, M., and Horrocks, L.: A Miniaturised Ultraviolet Spectrometer for Remote Sensing of SO_2 Fluxes: A New Tool for Volcano Surveillance, J. Volcanol. Geoth. Res., 119, 241–254, https://linkinghub.elsevier.com/retrieve/pii/S0377027302003566, 2003.

Galle, B., Johansson, M., Rivera, C., Zhang, Y., Kihlman, M., Kern, C., Lehmann, T., Platt, U., Arellano, S., and Hidalgo, S.: Network for Observation of Volcanic and Atmospheric Change (NOVAC)—A Global Network for Volcanic Gas Monitoring: Network Layout and Instru-

https://doi.org/10.5194/egusphere-2026-1387
Preprint. Discussion started: 24 March 2026

ment Description, J. Geophys. Res.-Atmos., 115, 2009JD011 823, https://agupubs.onlinelibrary.wiley.com/doi/10.1029/2009JD011823, 2010.

Goff, F., Love, S. P., Warren, R., Counce, D., Obenholzner, J., Siebe, C., and Schmidt, S. C.: Passive Infrared Remote Sensing Evidence for Large, Intermittent CO_2 Emissions at Popocatépetl Volcano, Mexico, Chem. Geol., 177, 133–156, https://linkinghub.elsevier.com/retrieve/pii/S0009254100003879, 2001.

Griffiths, P. R. and De Haseth, J. A.: Fourier Transform Infrared Spectrometry, no. 171 in Chemical Analysis, Wiley-Interscience, Hoboken, N.J, 2nd ed edn., 2007.

Hobbs, P. C.: Building Electro-Optical Systems: Making It All Work., John Wiley & Sons, 2 edn., 2009.

Judd, J. W.: Volcanoes: What They Are and What They Teach, vol. 35 of *The International Scientific Series*, D. Appleton and Company, New York, 1895.

Kern, C., Lübcke, P., Bobrowski, N., Campion, R., Mori, T., Smekens, J.-F., Stebel, K., Tamburello, G., Burton, M., Platt, U., and Prata, F.: Intercomparison of SO_2 Camera Systems for Imaging Volcanic Gas Plumes, J. Volcanol. Geoth. Res., 300, 22–36, https://linkinghub.elsevier.com/retrieve/pii/S0377027314002662, 2015.

Knapp, M., Kleinschek, R., Vardag, S. N., Külheim, F., Haveresch, H., Sindram, M., Siegel, T., Burger, B., and Butz, A.: Quantitative Imaging of Carbon Dioxide Plumes Using a Ground-Based Shortwave Infrared Spectral Camera, Atmos. Meas. Tech., 17, 2257–2275, https://amt.copernicus.org/articles/17/2257/2024/, 2024.

Love, S. P., Goff, F., Counce, D., Siebe, C., and Delgado, H.: Passive Infrared Spectroscopy of the Eruption Plume at Popocatépetl Volcano, Mexico, Nature, 396, 563–567, https://www.nature.com/articles/25109, 1998.

Löw, B. A., Kleinschek, R., Enders, V., Sander, S. P., Pongetti, T. J., Schmitt, T. D., Hase, F., Kostinek, J., and Butz, A.: A Portable Reflected-Sunlight Spectrometer for CO_2 and CH_4, Atmos. Meas. Tech., 2023.

Mori, T., Notsu, K., Tohjima, Y., and Wakita, H.: Remote Detection of HCl and SO_2 in Volcanic Gas from Unzen Volcano, Japan, Geophys. Res. Lett., 20, 1355–1358, https://agupubs.onlinelibrary.wiley.com/doi/10.1029/93GL01065, 1993.

Murata, K. J.: Occurrence of CuCl Emission in Volcanic Flames, Am. J. Sci., 258, 769–772, 1960.

Naughton, J. J., Derby, J. V., and Glover, R. B.: Infrared Measurements on Volcanic Gas and Fume: Kilauea Eruption, 1968, J. Geophys. Res., 74, 3273–3277, http://doi.wiley.com/10.1029/JB074i012p03273, 1969.

Notsu, K., Mori, T., Igarashi, G., Tohjima, Y., and Wakita, H.: Infrared Spectral Radiometer: A New Tool for Remote Measurement of SO_2 of Volcanic Gas., Geochem. J., 27, 361–366, http://www.jstage.jst.go.jp/article/geochemj1966/27/4-5/27_4-5_361/_article, 1993.

Oppenheimer, C., Francis, P., Burton, M., Maciejewski, A., and Boardman, L.: Remote Measurement of Volcanic Gases by Fourier Transform Infrared Spectroscopy, Appl. Phys. B-Lasers O., 67, 505–515, http://link.springer.com/10.1007/s003400050536, 1998.

Pyle, D. and Mather, T.: Halogens in Igneous Processes and Their Fluxes to the Atmosphere and Oceans from Volcanic Activity: A Review, Chem. Geol., 263, 110–121, https://linkinghub.elsevier.com/retrieve/pii/S000925410800538X, 2009.

Scott, S., Pfeffer, M., Oppenheimer, C., Bali, E., Lamb, O. D., Barnie, T., Woods, A. W., Kjartansdóttir, R., and Stefánsson, A.: Near-Surface Magma Flow Instability Drives Cyclic Lava Fountaining at Fagradalsfjall, Iceland, Nat. Commun., 14, 6810, https://www.nature.com/articles/s41467-023-42569-9, 2023.

Smekens, J.-F., Mather, T. A., Burton, M. R., Varnam, M., and Pfeffer, M. A.: Rapid Primary Sulfate Aerosol Generation Observed With OP-FTIR in the Eruptive Plume of the Fagradalsfjall Basaltic Eruption, Iceland, 2021, J. Geophys. Res.-Atmos., 129, e2023JD040 574, https://agupubs.onlinelibrary.wiley.com/doi/10.1029/2023JD040574, 2024.

Verhoogen, J.: New Data on Volcanic Gases; the 1938 Eruption of Nyamlagira., Am. J. Sci., 237, 656–672, 1939.